Pan, Rongliang; Hostikka, Simo; Zhu, Guoqing; Xu, Gang; Liu, Xin

Two-Dimensional Analysis on Ceiling Jet Temperature Characteristics in a Semicircular Tunnel

Published in:
Fire Technology

DOI:
10.1007/s10694-021-01185-z

Published: 01/03/2022

Two-dimensional analysis on ceiling jet temperature characteristics in a semicircular tunnel

Rongliang Pan [a, b, c] Simo Hostikka [c] Guoqing Zhu [a, b *] Gang Xu [a, b] Xin Liu [a, b]

[a] Jiangsu Key Laboratory of Fire Safety in Urban Underground Space（China University of Mining and Technology）, Xuzhou 221116, China

[b] School of Safety Engineering, China University of Mining and Technology, Xuzhou 221116, China

[c] Department of Civil Engineering, Aalto University, FI-00076 AALTO, Finland

Abstract

In order to reveal the evolution of ceiling jet temperature characteristics beneath curved ceiling in two-dimensional view, experimental and theoretical studies were conducted to analyze the vertical temperature profile and longitudinal temperature attenuation beneath a curved ceiling of a semicircular tunnel. The temperature profile was first measured from experiments carried out in the model-scale semicircular tunnel. The relationship between temperature and the horizontal positions is described by an empirical model. A formula describing the thickness of the thermal boundary layer is proposed, based on the vertical distribution of smoke temperature. An engineering model for the longitudinal attenuation of the gas temperature with different fire plume types at impingement region is established in terms of conservation equations. After validation, model predictions show a good agreement with trend proposed by former literature and the relative error of prediction is found to be within 10%. Two-dimensional prediction for temperature profile beneath semicircle ceiling centerline was proposed. It was noted that two-dimensional prediction model could predict majority of measured data within 20% relative error even though some fluctuation, which could be applied to the fire protection engineering in semicircular tunnel.

Keywords

Curved ceiling; Temperature profile; Thermal boundary layer; Longitudinal temperature attenuation; Two -dimensional temperature profile

Nomenclature

B	Wet perimeter of thermal layer (m)
c_f	Fanning friction factor
C_1, C_2, C_3, C_4, C_5	Constant obtained from experiments
C_p	Heat capacity of air (kJ/(kg.K))
h_c	Convective heat transfer coefficient (kW/(m^2.K))
h_{rad}	Radiative heat transfer coefficient (kW/(m^2.K))

* Corresponding author. School of Safety Engineering, China University of Mining and Technology, Xuzhou 221116, China
E-mail address: zgq119xz@cumt.edu.cn (Guoqing Zhu)

H	Ceiling clearance above fire source (m) (In this work, H=R)
l	Half width of tunnel (m)
L	Width of thermal boundary layer (m)
L_T	The vertical position from ceiling where $\triangle T/\triangle T_{max}(x)$ =1/e (m)
$\dot{m}$	Mass flow of entrained flow and thermal layer (kg/s)
$\dot{m}_e$	Mass flow of entrained flow (kg/s)
Pr	Prandtl Number
Q_{conv}	Convective heat loss from thermal layer to the ceiling (kW/m)
Q_{rad}	Radiative heat loss from thermal layer to the ceiling (kW/m)
R	The radius of tunnel (m)
Re	Reynolds number
Ri	Richardson number
s	Cross-section area of thermal boundary layer (m^2)
St	Stanton number ($St= h_c/(C_p\rho u)$)
T_e	Characteristic temperature of entrained layer (K) (In this work, $T_t= T_e$)
T_t	Characteristic temperature of thermal layer (K)
$T_{t,o}$	Characteristic temperature of thermal layer at the reference point x_o (K)
T_w	Temperature of concrete wall (K)
T_∞	Ambient temperature (K)
$\Delta T(x,z)$	Temperature rise at point with x from fire source and z from ceiling (K)
$\Delta T_{max}(x)$	Maximum temperature rise with the same horizontal distance from fire source (K)
ΔT_t	Characteristic temperature rise of thermal boundary layer (K)(In this work, $\triangle T_t=\triangle T_{max}$)
$\Delta T_{t,o}$	Characteristic temperature rise of thermal boundary layer at reference point (K)
u	Horizontal flow velocity of thermal layer (m/s)
x	Horizontal distance from fire source (m)
x_f	Horizontal location of the boundary between region II and III (m)
x_o	Horizontal distance from fire source to the reference point (In this work, x_o=3 m)
x_v	Distance between the virtual origin and the fire source (m)
z	Vertical position from ceiling (m)
Z_{max}	The vertical position from ceiling where $\triangle T/\triangle T_{max}(x)$ =1 (m) $Z_{max}=\delta(x)$ in this work

Greek symbols

γ	Coefficients in the Eq.13
$\delta(x)$	Thickness of thermal boundary layer at x (m)
ε	Coefficients in the Eq.13
ε_w	Emissivity of wall surface
ρ	Smoke density (kg/m^3)

1. Introduction

Semicircular tunnel is a common form of road and railway tunnels where the ceiling is formed as a semicircular structure. Differing from the tunnels with horizontal ceiling [1, 2], the semicircular tunnel has unique ceiling jet behavior because of its semicircular ceiling [3-9].

Specifically speaking, due to the unique geometry, ceiling jet with curved ceiling owns deeper thermal layer and less heat transfer with the surroundings compared to the flat ceiling, producing the higher temperature beneath ceiling[7-9]. In addition, curved ceiling forms a different smoke layer cross section, comparing with horizontal ceiling, resulting in the governing equations in horizontal ceiling could not be applied into semicircular tunnel directly[3]. Even though several works have been conducted to analysis the jet temperature characteristics under curved ceiling [4-6], proposed empirical models were established through dimensionless analysis from experimental data, lacking of government equations employment[4, 5]. The other semi-empirical models were proposed based on the governing equations, but evolution of smoke layer cross section and heat transfer were simplified in the governing equations[6]. In addition, existing literature on ceiling jet under semicircular ceiling has not analyzed temperature profile from two-dimensional view. In order to supplement the relevant theoretical research on ceiling jet in semicircular tunnel, in this study, the two-dimensional ceiling jet temperature distribution under the curved ceiling will be analyzed, which is the main characteristic parameter of a ceiling jet.

Numerous studies have focused on the temperature distribution of ceiling jet in tunnel fires. Alpert [10] conducted a series of fire experiments beneath a unconfined horizontal ceiling and established a longitudinal temperature distribution model. The formula is established by the axially symmetric temperature attenuation theory with combination of abundant tunnel fire experiments. Based on Alpert's work, Delichatsios [11] proposed a theoretical model for predicting the average temperature attenuation under horizontal ceiling, shown as follows:

$$\frac{\Delta T_{average}}{\Delta T_f}\left(\frac{l}{H}\right)^{1/3} = 0.49\exp\left[-6.67St\frac{x}{H}\left(\frac{l}{H}\right)^{1/3}\right] \tag{1}$$

where $\Delta T_{average}$, ΔT_f and l represent the average temperature difference between smoke and ambient, average temperature difference above fire location and the half width of the tunnel. x and H are the horizontal distance from fire source and tunnel height, respectively. In addition, St is the Stanton number, which will be explained in the following section. Delichatsios [11] ignored the heat loss from smoke layer to ceiling and air entrainment. Ingason et al [12] conducted full-size combustion experiments in the rectangular tunnel and established a semi-empirical model

$$\frac{\Delta T(x)}{\Delta T_{\max}} = 0.55\exp(-0.143\frac{x-x_v}{H}) + 0.45\exp(-0.024\frac{x-x_v}{H}) \tag{2}$$

The foundation of Eq. 2 is the heat balance of a smoke control volume at distance *x,* and virtual origin is employed to take into account the effect of flame extension under the ceiling. x_v is the distance between the virtual origin and the fire source, which could be expressed as follows:

$$x_v = \begin{cases} L_f - 10H, & L_f > 10H \\ 0, & L_f > 10H \end{cases} \tag{3}$$

where L_f is a corrected flame length. The model established by Ingason [12] can be applied to the conditions with flame extension beneath ceiling. However, the formula neglected the heat transfer between smoke layer and fresh air. Moreover, the equation was proposed to predict the longitudinal gas temperature attenuation in rectangular tunnel rather than semicircular tunnel. Based on theories above, Ye et al [13] predicted the longitudinal maximum temperature distribution in the rectangular tunnel,

$$\frac{\Delta T_t}{\Delta T_{t,o}} = \exp\left\{ -\frac{St}{\gamma(1-\varepsilon)H^{1-\varepsilon}}\left(x^{1-\varepsilon} - x_o^{1-\varepsilon}\right) - \frac{St}{l}(x - x_o) \right\} \tag{4}$$

where x_o is the horizontal distance from fire source to the reference point and $\Delta T_{t,o}$ represents the maximum temperature rise of thermal boundary layer at reference point. Reference point is employed as the starting point of ceiling jet region to be analyzed. In addition, constants γ and ε were obtained from experiments. Eq.4 proposed by Ye et al [13] could be applied to the tunnel with two sides sealed. Even though empirical models for the thickness of the thermal boundary layer were employed to establish the formula, it provides an accurate tool for analyzing the longitudinal temperature attenuation in rectangular tunnels.

In summary, equations proposed by former scholars focused on the ceiling jets in rectangular tunnel with horizon ceiling. The research on the jet behavior beneath curved ceiling is relatively rare and the theories established by the former scholars may not be applicable to semicircular tunnels with curved ceiling. because of different vertical temperature distribution and heat transfer with the surroundings[7, 14]. Different vertical temperature could result in the difference in the boundary between thermal layer and entrained layer, influencing the selection of control volume when establishing conservation equations. On the other hand, comparing with horizontal ceiling, heat transfer from ceiling jet to surroundings performs different due to contact surface with surroundings[15]. In order to establish accurate conservation equations when describing jet behavior under curved ceiling, it is necessary to analyze temperature profile and determine control volume firstly[10-12, 16].

In this work, a series of experiments with strong and thin plumes are carried out in the model-scale semicircular tunnel. Then the temperature profile, ceiling jet thickness and longitudinal temperature distribution beneath curved ceiling will be analyzed. Finally, a formula predicting two-dimensional temperature profile beneath curved ceiling centerline is proposed through experimental and theoretical analysis.

2. Experimental procedure

A model tunnel with semicircular ceiling (length of 20 m, radius of 0.75 m) was employed to simulate a road or railway tunnel with curved structure. The model tunnel was constructed of 15 cm thick concrete and equipped with several observation windows which were covered by fire-resistant glass, so that flame characteristics and smoke movement could be observed.

Froude scaling is widely used in tunnel fire research to describe the relation between the measured conditions in a reduced-scale experiment and their full-scale counterparts [17-20]. In this work, temperature, mass flow $\dot{m}$, and velocity u are measured in the model scale tunnel. Based on Froude scaling, these quantities can be expressed in full-scale as

$$\begin{aligned} T_F &= T_M \\ \frac{\dot{m}_F}{\dot{m}_M} &= \left(\frac{l^*_F}{l^*_M}\right)^{5/2} \\ \frac{u_F}{u_M} &= \left(\frac{l^*_F}{l^*_M}\right)^{1/2} \end{aligned} \tag{5}$$

where l^* is the length scale, and indices F and M refer to the full and model scales, respectively. Following the previous studies [21-24], a pool fire is used to produce the ceiling jet. Considering the model tunnel scale and previous burner dimensions [3, 25], a square pool (0.15 m×0.15 m), welded from 2 mm thick steel plates, was employed as the fire source in this study. Methanol, Ethanol and N-heptane were used as the fuel, leading to three different kinds of fire plumes. To ensure the consistency of the experiment, the same batch of fuel was employed throughout the study. As shown in Fig 1, the fire source was placed in the middle of the model tunnel. Six thermocouple trees were placed on the tunnel centerline with spacing of 1.0 m, starting from 3.0 m from the fire source. As shown in Fig 1(a), each tree had seven 0.2 mm thick K-type thermocouples with estimated response time of 1.0 s and positioned to capture the vertical temperature distribution observed by the previous literature [13, 16]. These thermocouples could measure temperatures of up to 1250 °C with accuracy of 0.01 °C. According to the former literature[26, 27], radiation effects are the most significant source of errors. Based on the reference[26-29], in this work, the uncertainty of thermocouples is estimated to be below 5% according to the maximum temperature measured, thermocouple geometry and estimated velocity of smoke.

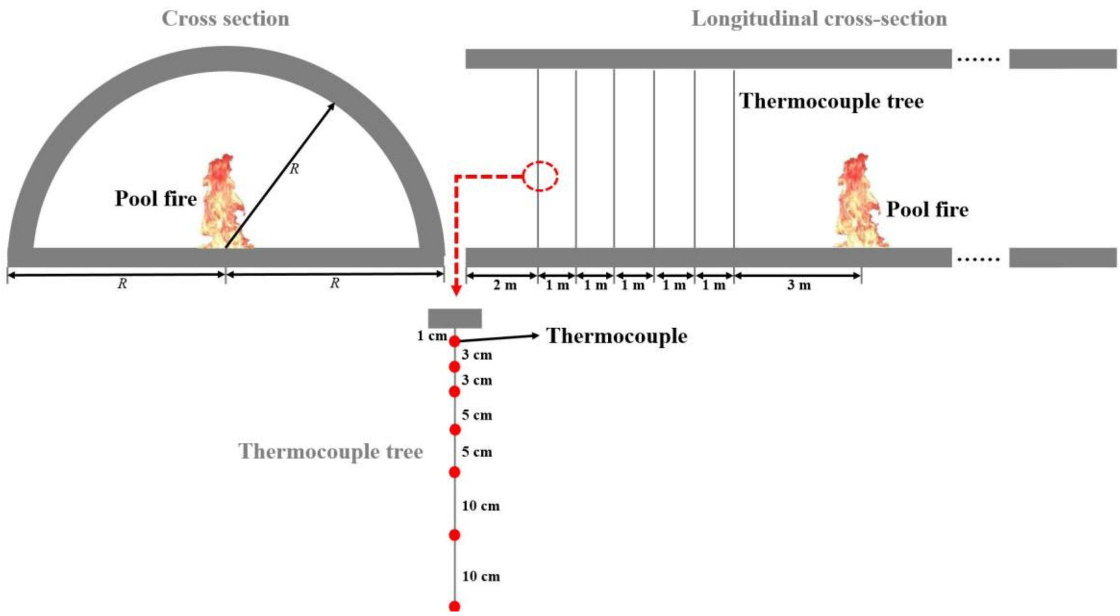

(a) Arrangement of thermocouple trees

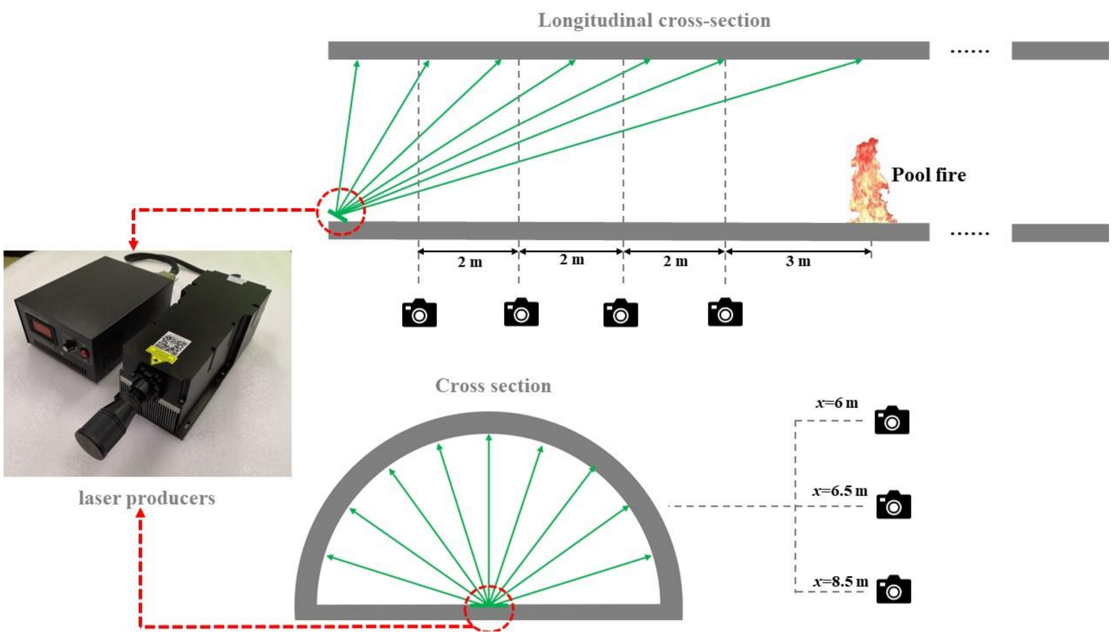

(b) Arrangement of laser sheet and HD camera

Fig 1 Experimental platform layout. Radius R = 0.75 m.

As shown in the Fig 1(b), a pair of laser producers with power of 10 W was used to create sheets of light to image jet movement beneath the semicircular ceiling. One was to produce longitudinal laser sheet and the other was to create transverse laser sheets (x=6, 6.5, 8.5 m). As for the transverse laser sheets, they were obtained in three repeated experiments, mentioned in the following. The laser irradiation angle was 120° with line thickness of 1.5 mm. The laser transmitters were insulated from heat to ensure their normal operation in the model tunnel. In addition, HD camera was installed outside the tunnel to record the flame shape and jet movement during the experiments, and the camcorder recorded videos at 20 frames per second.

Experiments were conducted with two sides open and tests with one fuel were repeated three times to quantify the random component of the experimental error. The mean and standard deviations of the ambient temperatures were 24.1 ± 0.3 °C for N-heptane tests, 28.3 ± 0.9 °C for ethanol tests, and 26.2 ± 0.2 °C for the methanol tests.

3. Experimental observations, theoretical analysis and discussion

3.1 Temperature profile

Taking the experiments with N-heptane as an example, a two-dimensional field of the gas temperature was constructed at time 600 s from ignition. The resulting temperature field is shown in Fig 2, where the horizontal axis indicates the distance along the tunnel from the fire source. At 3.0 m distance, the ceiling jet temperature rise is more than 130 K, and it decreases to range 75 to 80 K at 8.0 m. The vertical position of the maximum temperature seems to decrease with increasing distance from the source, but the boundary of smoke layer (obtained from laser visualization picture) seems develop in a non-monotonic manner.

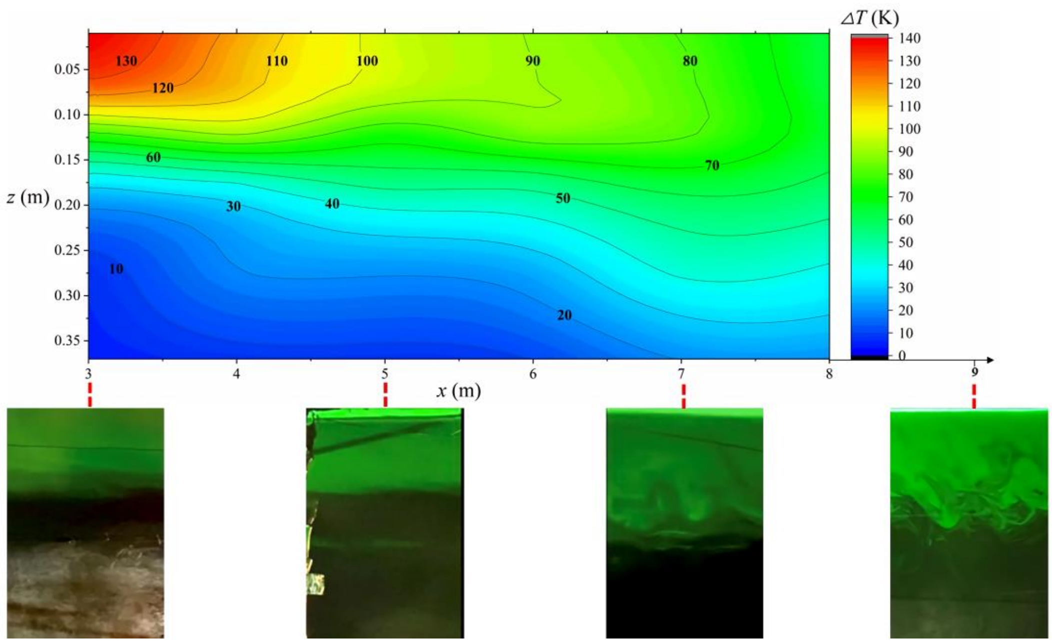

Fig 2. Temperature field (top) and laser visualization picture at positions x = 3, 5, 7 and 9 m for N-heptane fire.

The temperature development along the tunnel is influenced by the heat transfer between ceiling jet and the tunnel surface, and the cooling due to the gas entrainment from the lower layer. The role of the gas entrainment can be evaluated from the laser visualization pictures shown in Fig 2. Close to the impingement point (x = 3 and 5 m), the smoke layer interfaces are relatively flat, which means there is only little mass exchange between smoke layer and cold air. As a result, the convective heat transfer due to the gas entrainment is rare and it is not hard to distinguish smoke layer from cold air layer by temperature field. As the horizontal distance increases (x = 7 m), shear-induced vortices appear at the interface, and at x= 9 m, the interface seems very turbulent. The convective heat transfer due to the gas entrainment perform more remarkable. Due to smoother temperature gradient at bottom, it becomes hard to distinguish smoke layer by temperature field. On the other hand, heat transfer from smoke layer to ceiling always play a significant role. With moving of smoke layer, the total heat loss to ceiling surface accumulates, leading to the more and more obvious temperature gradient at top, seen in the Fig.2.

The detailed temperature values of the temperature rise for each fuel are shown in Fig 3. Fig 3 was drafted by the experimental data obtained in steady state. The time reaching steady state of each fuel was listed in the Table 1 as well as corresponding HRR. With same fuel, all the data was selected with same time.

Table1 Summary of the time reaching steady state and corresponding HRR

Test	Fuel	Time reaching steady state /s	HRR /kW
Tests 01~03	N-heptane	600	35.8
Tests 04~06	Ethanol	582	16.5
Tests 07~09	Methanol	510	10.1

As shown in the Fig.3, even though maximum temperature near fire source is close to ceiling, on the whole, temperature follows a top-hat distribution where temperature rises from ceiling to the maximum value and then drops down towards ambient temperature. Moreover, vertical distribution varies with increasing of horizontal distance from fire source.

As the temperatures were measured at discrete heights, the actual position of the maximum temperature can appear somewhere between the measurement points. The maximum temperature rise ΔT_{max} and its height z_{max} were thus obtained from quadratic polynomials fitted to the measured maximum temperature and two nearest values, separately at each horizontal distance [30-32]. In addition, the value of $\Delta T_{max}/e$ and its position were obtained through the same method. The fitted and measured data points were shown in the Fig.3.

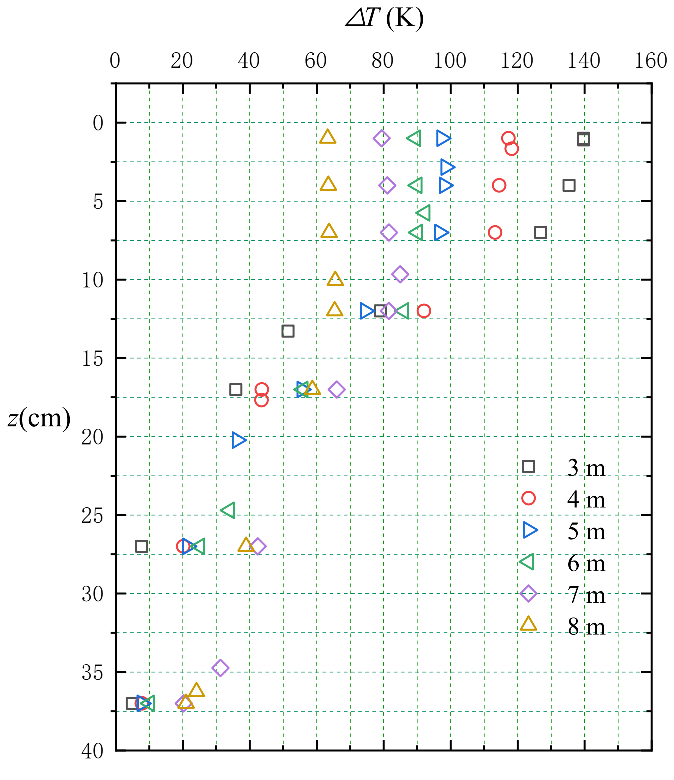

(a) N-heptane

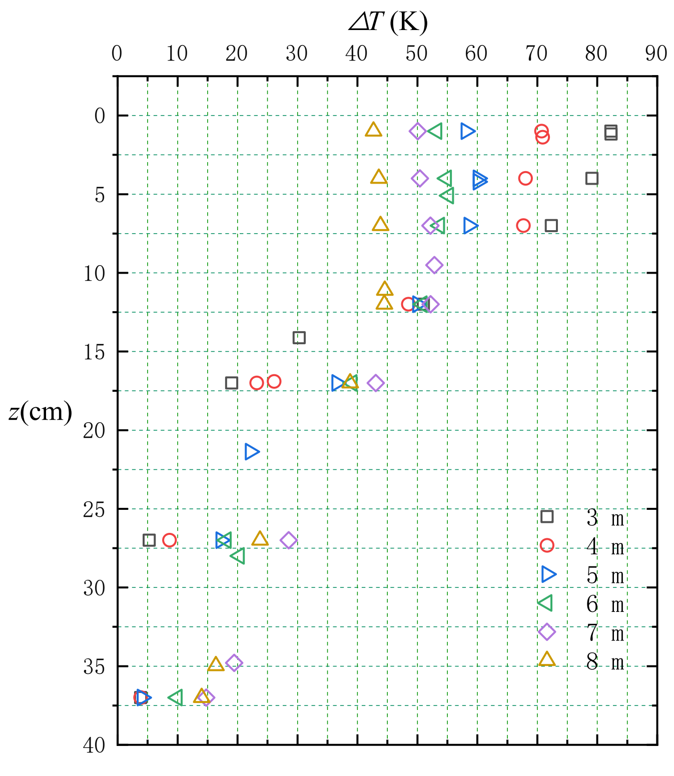

(b) Ethanol

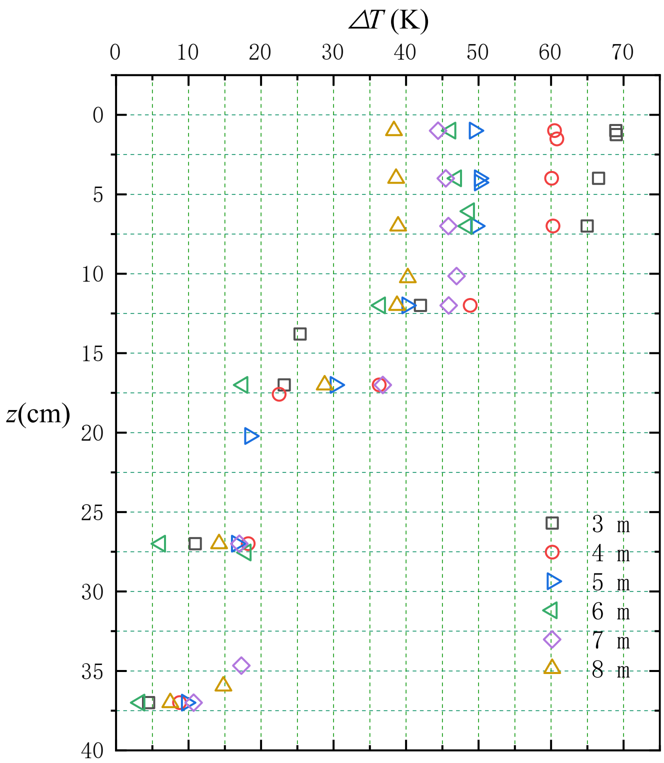

(c) Methanol

Fig. 3 Fitted and measured temperature increase at different heights and distances from the fire source with different fuels.

Referring to former literature [30-33], the relationship between temperature profile and horizontal positions could be unified as

$$\frac{\Delta T}{\Delta T_{\max}} = C_1\left(\frac{z}{L_T} + C_2\right)^{C_3} \exp\left(C_4 \frac{z}{L_T}\right) \tag{6}$$

This equation states that the non-dimensional temperature rise $\Delta T/\Delta T_{max}$ only depends on the non-dimensional vertical distance from the ceiling z/L_T, where L_T (Gaussian thermal thickness) represents the vertical position where $\Delta T/\Delta T_{max}$ =1/e. Fig 4 shows the non-dimensional temperature profiles, indicating independence from HRR and horizontal position. The red area shown in Fig 4 represents 10% relatively error, containing almost all the data points. Coefficients C_1, C_2, C_3 and C_4 are determined by nonlinear analysis from the experiments. The presented models were previously derived by Motevalli and Oka [30, 33] in their model scale experiments, and the coefficients of these three models are shown in Table 2.

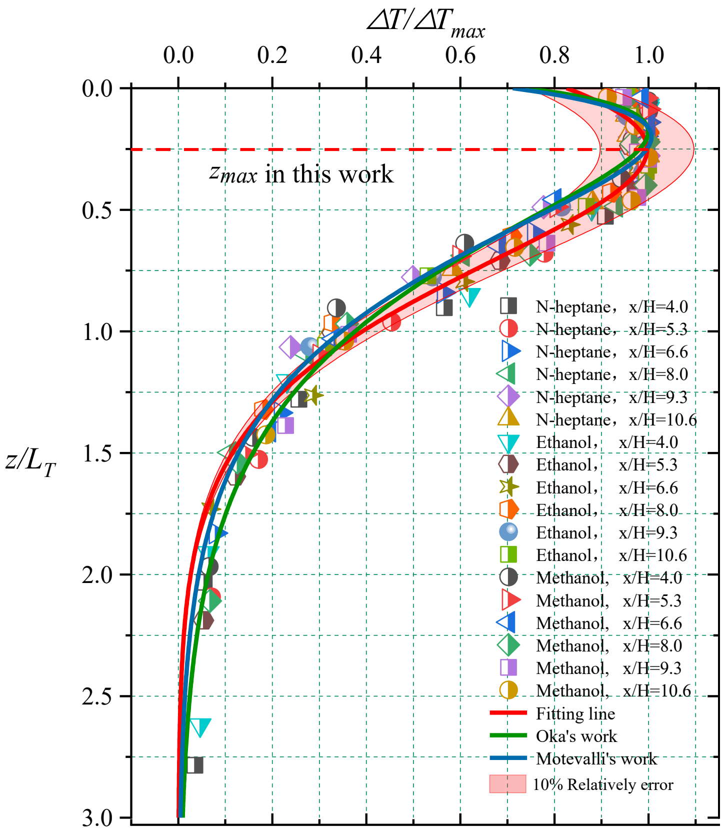

Fig.4 Non-dimensional temperature profiles beneath ceiling centerline with several HRRs in curved tunnel

A comparison between fitting lines obtained in this work and the former works is also shown in Fig 4. Even though the current model (red line) shows a good agreement with the ones put forward by Motevalli [33] and Oka[30, 31] (green and blue lines) when $z > z_{max}$, some difference exists when $0 < z < z_{max}$. Specifically, data predicted by red line as well as experimental data shows lower temperature gradient than Motevalli and Oka's data in this region. In other words, the heat loss transfer in the region $0 < z < z_{max}$ under curved ceiling is lower than that under horizontal ceiling. Two factors may contribute to this behavior:

① Due to the curved geometry, ceiling jet with same thickness has smaller touching boundary with environment, comparing with that under horizontal ceiling.

② In ceiling jet region, from Reynold/Colburn analogy, the heat transfer coefficient at the ceiling h could be expressed as follows[34],

$$\frac{h}{\rho v C_p} = \mathrm{Pr}^{-2/3}\frac{f}{2} \tag{7}$$

where ρ, v and C_p represent the density, average velocity and specific heat of ceiling jet. Moreover, Pr and f are the Prandtl number and friction factor of ceiling, respectively. For the same ceiling surface and jet with same properties, the Prandtl number, density, specific heat and friction factor could be regarded as constant in this work[35]. As a result, based on the Eq.7, lower average velocity v responds to the lower heat transfer coefficient at the ceiling h. Fire plume impinges ceiling centerline (highest point) and then produces the ceiling jet. Due to curved geometry, radial ceiling jet flows against buoyancy when moving to sidewall. So average velocity v beneath curved ceiling is slower than that under horizontal ceiling, resulting in the lower heat transfer coefficient h of ceiling jet under the curved ceiling. Thus, the temperature gradient with $0 < z < z_{max}$ under curved ceiling is much lower.

Table 2 Estimated values of coefficients to describe temperature profile at each inclination angle of the ceiling

	C_1	C_2	C_3	C_4
This work	3.49	0.745	4.896	-4.91
Motevalli	4.24	0.0940	0.755	-2.57
Oka	3.03	0.0660	0.519	-2.12

3.2 Thermal boundary layer

In order to analyze the longitudinal maximum temperature distribution, thermal boundary layer was employed when writing governing equations.

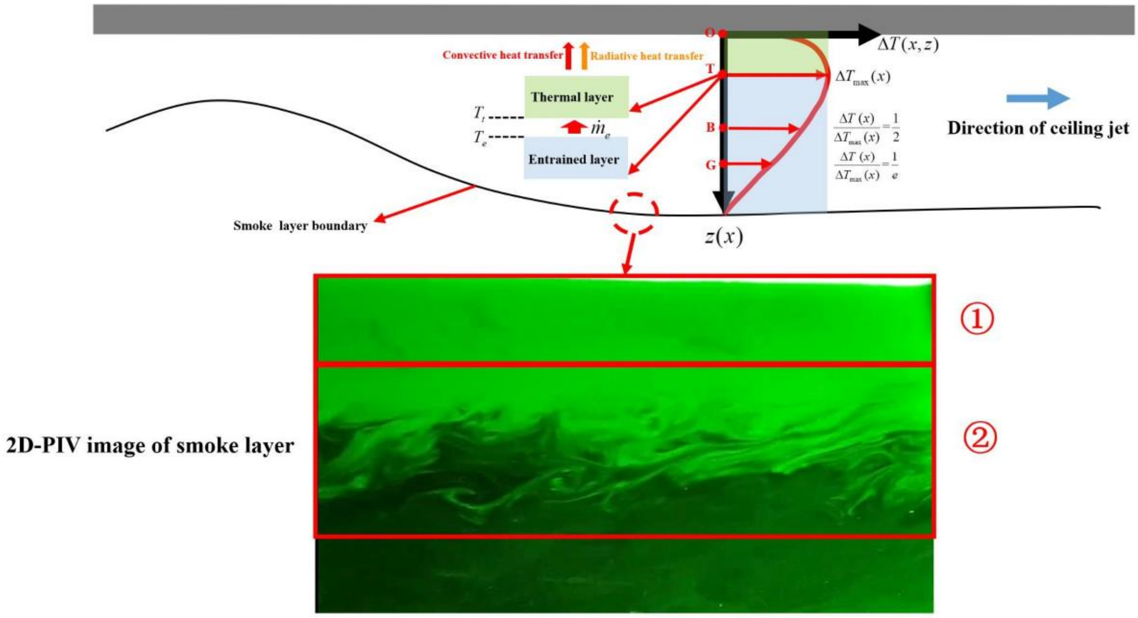

Fig. 5 Mechanism of jet movement under curved ceiling (①: upper smoke layer, ②: lower smoke layer)

As shown in the Fig 5, Point T is the position of maximum temperature and point B is the position where the temperature increase is the half of maximum value. In addition, point G represents position where the temperature increase is the 1/e of maximum value. Vertical length from point O to G is the Gaussian thermal thickness L_T, which mentioned in section 3.1. Several scholars have defined the ceiling jet thickness through temperature profile. Earlier, Oka [16] defined length between point O and B as the ceiling jet thickness. While in Ye's work[13], length from point O to T was defined as the ceiling jet thickness (thermal boundary layer thickness in his work). Seen in the Fig.5, the upper smoke layer (① in the Fig 5) was relatively flat comparing with lower smoke layer (② in the Fig 5). It could be noted that there were lots of vortexes in the lower smoke layer, especially in the interface between smoke layer and cold air layer. A large number of vortexes means that violent exchange of heat and mass transfer, resulting in unstable characteristic in lower smoke layer [19]. In order to make it easier for governing equations establishment, upper smoke layer (① in the Fig 5) was worthy of being selected as the control volume because of stable state in it. In addition, according to Section 3.1 and seen in Fig 4, vertical temperature gradient with $0 < z < z_{max}$ is tiny, which could be ignored when establishing conservation equations. As a result, with reference to Ye's work[13], boundary where maximum temperature value in vertical direction was defined as the thermal boundary and region above the boundary was regarded as thermal layer (green area in Fig.5). Seen in the Fig 5, with jet movement along ceiling, entrained layer (blue area) is entrained into the thermal layer (green area) as well as heat transfer between them. Meanwhile, heat transfer from thermal layer to ceiling plays a significant role, which is composed by radiative and convective heat flux.

Several scholars have proposed approximate formula about thickness of thermal boundary layer [11, 16, 36-38]. Referring to their work, in the attenuation region (far from impingement region), the thermal boundary layer thickness $\delta(x)$ could be mainly influenced by tunnel geometry, relative position to the fire source, ventilation at both sides of the tunnel and fire source location. Considering that fire source location remained the same in experiments and both sides of tunnel were open without longitudinal ventilation, the relationship among them could be concluded as follows:

$$f\left[\delta(x), x, H, l\right]=0 \tag{8}$$

Where $\delta(x)$ represented the thickness of thermal boundary layer, x, H and l were horizontal distance from fire source, ceiling clearance above fire source and half width of tunnel, respectively. Considering that the width of curved tunnel is not a constant value, half width of tunnel l was defined to be the half of maximum width in tunnel. Based on the dimensional analysis, Eq.8 could be written as,

$$\frac{\delta(x)}{H} = f\left(\frac{x}{H}, \frac{l}{H}\right) \tag{9}$$

On the basis of Eq.9, two alternative correlations for the thermal boundary layer thickness were proposed in earlier work [11, 13, 16, 39], shown as follows:

$$\begin{cases} \frac{\delta(x)}{H} = a\left(\frac{x}{H} - \frac{l}{H}\right) + b\left(\frac{l}{H}\right)^d \\ \frac{\delta(x)}{H} = c\left(\frac{l}{H}\right)^d \end{cases} \quad (a)$$
$$\frac{\delta(x)}{H} = \gamma\left(\frac{x}{H}\right)^{\varepsilon} \quad (b) \tag{10}$$

The form difference reflected in the Eq.10 is resulted from the development of ceiling jet. Referring to the former literature[11, 16, 35], ceiling jet could be divided into three regions based on the horizontal distance from fire source, shown in the Fig.6: ①Region I, axisymmetric radial ceiling jet. ②Region II, one-dimensional shooting flow. ③Region III, one-dimensional critical flow, where Ri=1[11]. Richardson number Ri is defined as the ratio of buoyancy force to inertia force[35, 40]. Eq.10(a) and Eq.10(b) were both proposed to describe thickness in the Region II and III. Eq.10(a) could be expressed in two forms according to the different regions. On the other hand, Eq.10(b) was employed to predict thickness approximately regardless of Region II and III. Seen in Eq.10, a, b, c, γ and ε were assumed as constant, which could be obtained from experiments.

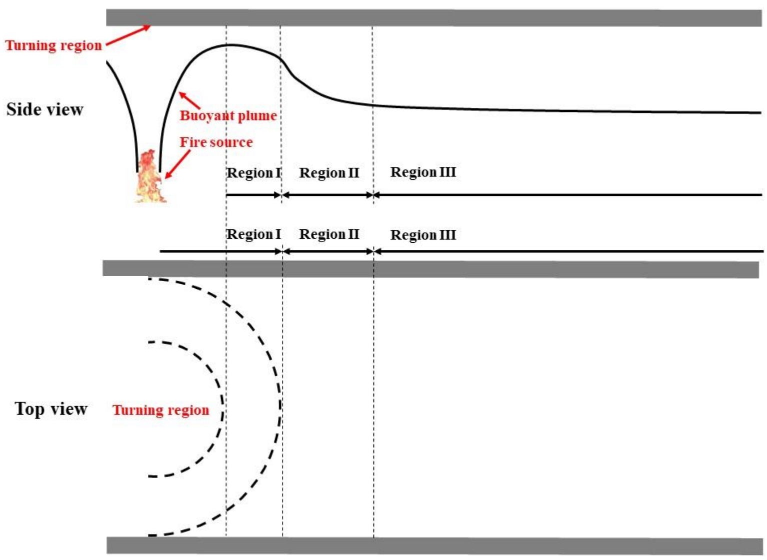

Fig. 6 Regions in the ceiling jet

It is reported that the boundary between Region I and II could be regarded as the half of tunnel width l [11, 35, 41]. Thus, temperature attenuation to be discussed mainly concentrate in the Region II and III because of 3 m≤x≤9 m.

Eq.10(a) describes the thickness in Region II and III, which was employed in Oka's work[16]. In Oka's prediction models, the correlations for the thermal boundary layer thickness were proposed as below,

$$\begin{cases} \dfrac{\delta(x)}{H} = 0.0842(\dfrac{x}{H} - \dfrac{l}{H}) + 0.152(\dfrac{l}{H})^{-1/3}, \text{Region II} \\ \dfrac{\delta(x)}{H} = 0.248(\dfrac{l}{H})^{-1/3} \qquad , \quad \text{Region III} \end{cases} \tag{11}$$

Even though earlier work defined interfaces with half maximum temperature as thermal boundary layer, the evolution law of *δ(x)/H* will not be influenced by the definition. Based on the Eq.11, it is found that boundary layer (ceiling-jet) thickness increases with accumulation of distance from the fire source in Region II and then remains almost constant in Region III. Delichatsios [11] also put forward similar correlation in Region III, which is expressed as $\delta(x)/H = 0.15(l/H)^{-1/3}$. Ye et al [13] employed the form of Eq.10(b) to describe thermal boundary layer thickness, shown as follows.

$$\frac{\delta(x)}{H} = 0.00116(\frac{x}{H})^{0.768} \tag{12}$$

Ye et al [13] defined the layer with the maximum temperature as thermal boundary layer, which is the reference of the definition in this work. Seen in the Eq.12, the predicted *δ(x)/H* increases slightly regardless of Region II and III. With reference to former works [11, 13, 16]and Eq.10, data estimated from experiments and empirical models in this work as well as Eq.12 are reflected in the Fig.7,

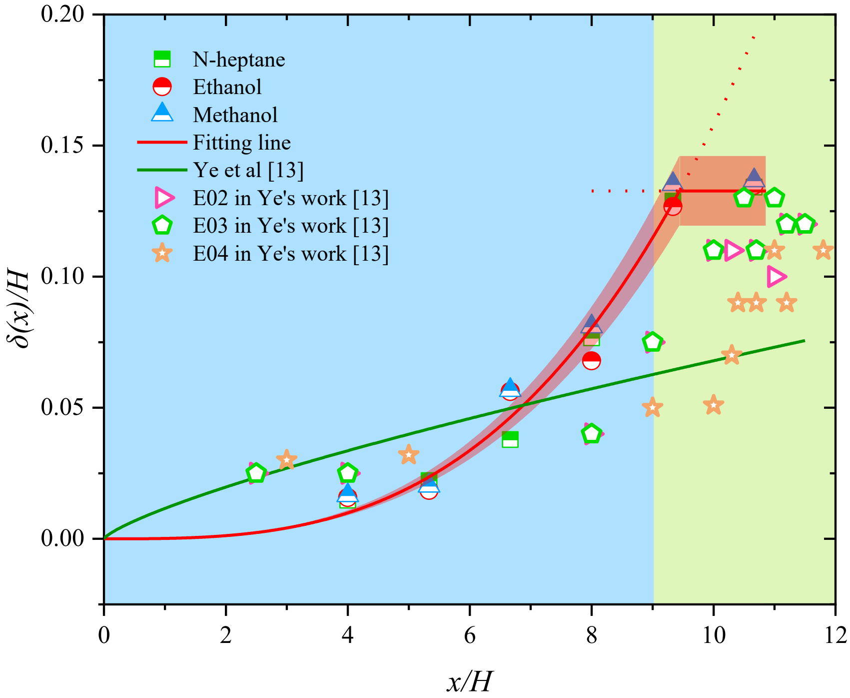

Fig. 7 Empirical model for thermal boundary layer thickness beneath curved ceiling

As shown in the Fig. 7, the relationship between *δ(x)/H* and *x/H* could be expressed with reference to the two alternative correlations in Eq.10. The new correlation was expressed in the Eq.13 and coefficients in the Eq.13 were determined based on the experimental data, shown in the Table.3

$$\frac{\delta(x)}{H}=\begin{cases}\gamma\left(\dfrac{x}{H}\right)^{\varepsilon} & \text{Region II} \quad (x/H<9)\\ c\left(\dfrac{l}{H}\right)^{-1/3} & \text{Region III} \quad (x/H\geq 9)\end{cases} \tag{13}$$

Seen in the Fig.7, the boundary between Region II and III is defined as *x/H*=9. Even though the boundary was determined by experimental data, it could still find reference from work proposed by Ye et al[13, 42]. In their work, the ceiling jet was produced by evolution of *δ(x)/H* performing two distinct stages and the boundary is around *x/H*≈10, which is similar with that in this work.

Table 3 Coefficients in the Eq.13

γ	ε	c
0.000149	3.02	0.130

In terms of Ye's model (green line), predicting line performs an increasing trend which is similar to data points. But the model could not predict *δ(x)/H* accurately, especially in the Region III. As shown in the Fig.7, data points from Ye's work [13] were employed to make comparison with work. It is obvious that values of $\delta(x)/H$ remains stable after $x/H\approx10$. Ye's model (green line) obtained from these data points could not perform well in this region. On the other hand, because of the thermocouple arrangement [13, 42], maximum temperature measured may not the actual value, which means the boundary position determined by raw temperature data may have the deficiencies in accuracy.

In a sum, based on the reference and experiments in this work, it could be inferred that evolution of $\delta(x)/H$ performs two distinct stages with increasing of x/H. It is necessary to describe thermal layer thickness in two forms of formula.

3.3 Longitudinal maximum temperature attenuation beneath curved ceiling

To establish the prediction formula, it is important to choose the appropriate control volume to develop conservation equations. As a reference, three transverse view laser visualization pictures with x=6, 6.5 and 8.5 m were shown in the Fig 8. It was shown that the low boundary of smoke layer beneath curved ceiling presented a slight circle, especially at the transverse ends. Seen in the Fig 8, the red lines were approximate horizontal boundary in this study. There was slight difference between factual and approximate line under the middle and edge ceiling. But the low boundary could be assumed as horizontal, which is accepted in engineering.

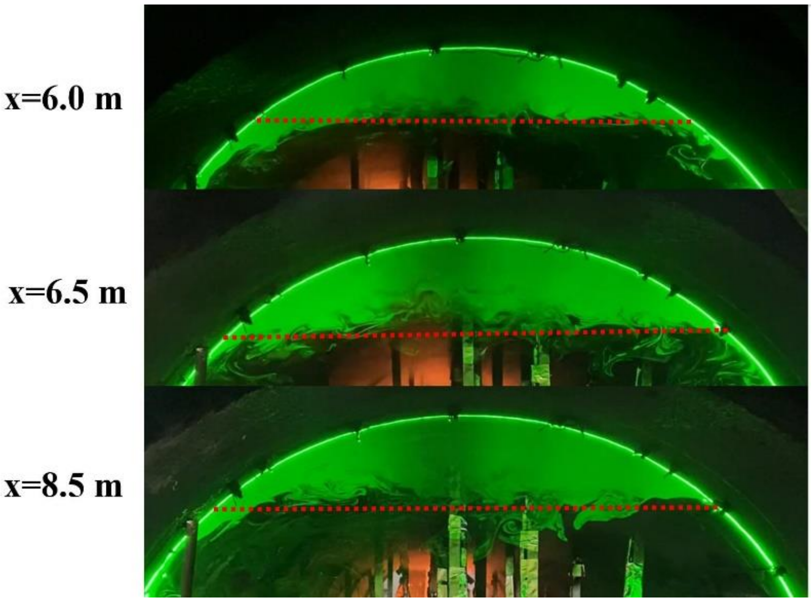

Fig. 8 Transverse view laser visualization pictures with x=6, 6.5 and 8.5 m

Seen in the Fig.5, the layer where $\Delta T/\Delta T_{max}$ =0 could be defined as smoke boundary. According to the former literature [42], interfaces where $\Delta T/\Delta T_{max}$=1, 0.8, 0.5 and 0.2 perform a great consistency and the distance between these interfaces remains stable regardless of position.

Thus, it could be inferred that evolution of smoke layer thickness is consistent with that of thermal boundary layer. Based on this assumption, the lower boundary of thermal layer beneath curved ceiling could also be regarded to be horizontal. Moreover Hu [43] once proposed the similar assumption when analyzing the temperature in smoke layer. To simplify the prediction models, control volume for thermal boundary layer was expressed in the Fig 9.

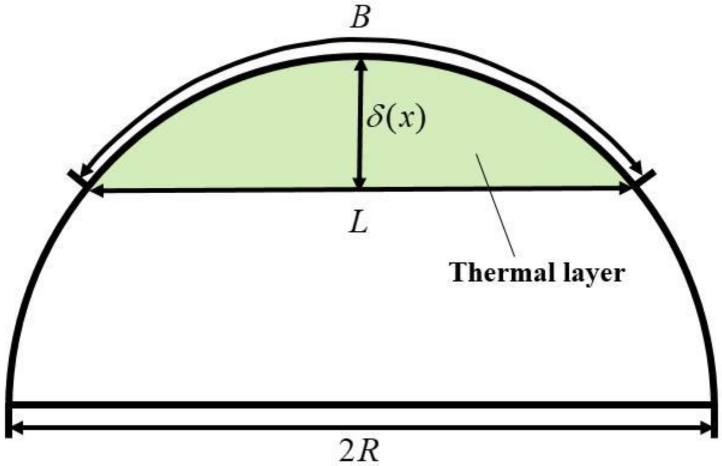

Fig. 9 Schematic diagram of thermal boundary layer beneath curved ceiling (Cross section)

L and B represented the width of thermal boundary layer and wet perimeter of thermal layer, respectively. They were expressed as follows:

$$L = 2\sqrt{\delta(x)(2R - \delta(x))} \tag{14}$$

$$B = 2R\arcsin(\frac{L}{2R}) \tag{15}$$

Thus, the cross-section area of thermal boundary layer s shown as green area in Fig 9 was described on the basic of Eqs.14 and 15,

$$s = \frac{R(B - L) + L\delta(x)}{2} \tag{16}$$

According to the derived equation Eq.A8 in the Appendix, the formula of wet perimeter B and cross-section area s of thermal boundary layer may increase the complexity of the model when x/H<9. On the basic of Liu's work[44], Eq.16 could be approximated by the following formula,

$$s \approx \frac{\pi R\delta(x)}{2} \tag{17}$$

Moreover, the Eq.15 was fitted as follows,

$$B \approx 0.43R + 4.5\delta(x) - \frac{2.7}{R}(\delta(x))^2 + \frac{0.9}{R^2}(\delta(x))^3 \tag{18}$$

If x/H < 9, Eqs. 17-18 and 13 are substituted into Eq.A8; if $x/H \geqslant$ 9, Eqs.15-16 and 13 are substituted into Eq. A8. Then Eq. A8 is integrated from x to x_o. Considering $\varepsilon \neq 1$ in the Eq.13 and H=R, the prediction equations were established.

$$\begin{cases} \dfrac{T_t - T_\infty}{T_{t,o} - T_\infty} = \exp(f(x) - f(x_o)) \\ f(x) = -\dfrac{(h_c + h_{rad})}{C_p \rho u \pi}\left[\dfrac{43x}{50\gamma(1-\varepsilon)R(\frac{x}{R})^\varepsilon} + \dfrac{9x}{R} - \dfrac{27\gamma x(\frac{x}{R})^\varepsilon}{5R(1+\varepsilon)} + \dfrac{9\gamma^2 x(\frac{x}{R})^{2\varepsilon}}{5R(1+2\varepsilon)}\right] \quad x/H < 9 \\ f(x) = -\dfrac{(h_c + h_{rad})}{C_p \rho u}\left[\dfrac{2R\arcsin(\sqrt{c(\frac{l}{R})^d(2-c(\frac{l}{R})^d)})}{(cR^2(\frac{l}{R})^d - R^2)\sqrt{cR(\frac{l}{R})^d(2R - cR(\frac{l}{R})^d)} + R^2\arcsin(\sqrt{c(\frac{l}{R})^d(2-c(\frac{l}{R})^d)})}\right]x \quad x/H \geq 9 \end{cases} \tag{19}$$

In Eq.19, the $T_{t,o}$ was the characteristic temperature of thermal layer at the reference point x_o. Considering that requirement of governing equations in Appendix (ceiling jet moves directly along longitudinal of tunnel and no flame exists in the smoke layer), the point where x=3 m was employed to be the reference point in this work. The $h_c/(C_p\rho u)$ is equal to the Stanton number St. In terms of $h_{rad}/(C_p\rho u)$, it could be transformed by the relation between radiative and convective heat transfer coefficients at the ceiling. The relationship is expressed as follows [45]:

$$h_{rad} / h_c = 3\varepsilon_w (T_t - T_w)^{-0.3} \tag{20}$$

Thus, the $h_{rad}/(C_p\rho u)$ could be written as:

$$\frac{h_{rad}}{C_p \rho u} = \frac{3\varepsilon_w (T_t - T_w)^{-0.3} h_c}{C_p \rho u} = 3\varepsilon_w (T_t - T_w)^{-0.3} St \approx C_5 St \tag{21}$$

Seen in the Eq.20, $3\varepsilon_w (T_t - T_w)^{-0.3}$ is not sensitive to the (T_t-T_w). As a result, $3\varepsilon_w (T_t - T_w)^{-0.3}$ with the same condition could be assumed as a constant C_5. Thus the Eq.19 could be expressed as:

$$\frac{\Delta T_l}{\Delta T_{l,o}}=\begin{cases}\exp\left\{\begin{aligned}&\frac{St(1+C_5)}{\pi}\left[\frac{43x_o}{50\gamma(1-\varepsilon)R(\frac{x_o}{R})^{\varepsilon}}+\frac{9x_o}{R}-\frac{27\gamma x_o(\frac{x_o}{R})^{\varepsilon}}{5R(1+\varepsilon)}+\frac{9\gamma^2x_o(\frac{x_o}{R})^{2\varepsilon}}{5R(1+2\varepsilon)}\right]\\&-\frac{St(1+C_5)}{\pi}\left[\frac{43x}{50\gamma(1-\varepsilon)R(\frac{x}{R})^{\varepsilon}}+\frac{9x}{R}-\frac{27\gamma x(\frac{x}{R})^{\varepsilon}}{5R(1+\varepsilon)}+\frac{9\gamma^2x(\frac{x}{R})^{2\varepsilon}}{5R(1+2\varepsilon)}\right]\end{aligned}\right\} & x/H<9\\ \exp\left\{\begin{aligned}&\frac{St(1+C_5)}{\pi}\left[\frac{43x_o}{50\gamma(1-\varepsilon)R(\frac{x_o}{R})^{\varepsilon}}+\frac{9x_o}{R}-\frac{27\gamma x_o(\frac{x_o}{R})^{\varepsilon}}{5R(1+\varepsilon)}+\frac{9\gamma^2x_o(\frac{x_o}{R})^{2\varepsilon}}{5R(1+2\varepsilon)}\right]\\&-\frac{St(1+C_5)}{\pi}\left[\frac{43x_f}{50\gamma(1-\varepsilon)R(\frac{x}{R})^{\varepsilon}}+\frac{9x_f}{R}-\frac{27\gamma x(\frac{x_f}{R})^{\varepsilon}}{5R(1+\varepsilon)}+\frac{9\gamma^2x_f(\frac{x_f}{R})^{2\varepsilon}}{5R(1+2\varepsilon)}\right]\\&-St(1+C_5)(x-x_f)\left[\frac{2R\arcsin(\sqrt{c(\frac{l}{R})^d(2-c(\frac{l}{R})^d)})}{(cR^2(\frac{l}{R})^d-R^2)\sqrt{cR(\frac{l}{R})^d(2R-cR(\frac{l}{R})^d)}+R^2\arcsin(\sqrt{c(\frac{l}{R})^d(2-c(\frac{l}{R})^d)})}\right]\end{aligned}\right\} & x/H\ge 9\end{cases} \tag{22}$$

Where x_f represented the horizontal location of the boundary between region II and III. Referring study in section 3.2, x_f was regarded as 7 m. In order to obtain the St number, the analysis is expected to be divided based on the fire plume types impingement regions (continuous flame, intermittent flame and plume). It is reported that Stanton number St has a relationship with Prandtl Number Pr and fanning friction factor c_f[35, 46], described as follows:

$$St=\frac{c_f/2}{1.07+12.7(Pr^{2/3}-1)\sqrt{c_f/2}} \tag{23}$$

Moreover, fanning friction factor c_f could be expressed as[35]:

$$c_f=\frac{1}{4\left\{1.81\lg\left[\frac{6.9}{Re}+(\frac{f}{3.7D})^{1.11}\right]\right\}^2} \tag{24}$$

Where Re and f/D represent Reynolds number and relative roughness of the tunnel surface, respectively. Furthermore, f and D are the roughness of the surface and hydraulic diameter of the tunnel. Considering that experiments were conducted in the same tunnel, relative roughness of the tunnel surface could be regarded as the same value. On the other hand, fire plume types in impingement region may cause the difference in the Reynolds number. For example, Reynolds number with extension flame in the impingement region have a little higher record than that without extension flame (plume) in the impingement region. Based on the Eqs.23-24, it could be inferred that St with extension flame (continuous flame) beneath ceiling has a little higher value than those with little (intermittent flame) or no (plume) extension flame beneath the ceiling, which has been proved by Ye et al[13].

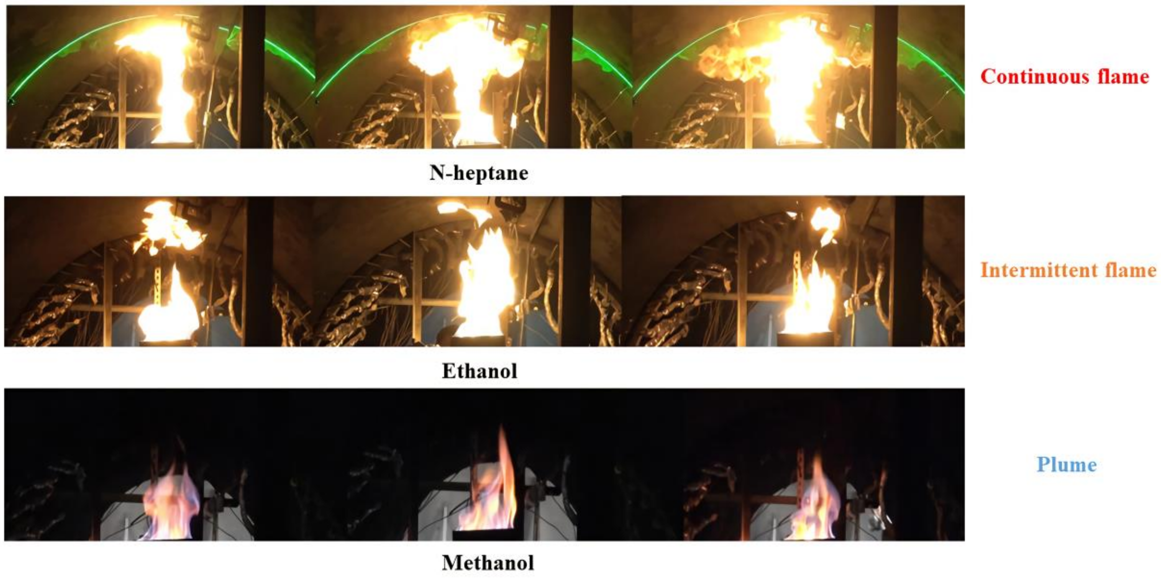

Fig. 10 Fire plume types at the impingement region (Methanol, Ethanol and N-heptane)

Seen in the Fig.10, fire plume produced by three kinds of heat release rates (N-heptane > Ethanol > Methanol) turns out to be different at the impingement region. According to the literature [47] and experimental outputs, higher heat release rate corresponds to higher flame height, which has more possibility to produce the flame extension beneath ceiling. Obviously, employing Methanol, the fire plume at the impingement point is almost the plume. When using Ethanol, there were intermittent flame existing under ceiling, proving intermittent flame region at the impingement point. As for the N-heptane, after impingement, stable flame extension happened under the ceiling. Therefore, fire plume type at the impingement region is regarded as the continuous flame.

Based on the experimental data, Stanton number St (continuous flame, intermittent flame and plume) is expected to be obtained through maximum temperature beneath curved ceiling at several points (x=4, 6 and 8 m). In this work, R=0.75 m, and the values of γ, ε, c and d would be obtained from Eq.13 as well as Table 3. As for the C_5, according to the Eq.21, ε_w and $(T_t\text{-}T_w)$ should be determined firstly. Based on the reference[45, 48, 49], the emissivity of wall could be equal to that of black soot, which changes slightly around 0.96 when the temperature is in the range of 323–1273 K.

Referring to the temperature data obtained from experiments, $(T_t\text{-}T_w)$ varies from 139.6 K to

38.7 K and C_5 changes from 0.65 to 0.96 based on Eq.21. In order to simplify the models, average value was employed to unify the C_5 based on the former work [50]. This methos is averaging values calculated from each temperature data (x=3,4,5,6,7 and 8 m) in each test (Test 01~09). The averaged value could reflect the concentration range of all the data. Based on Froude number scaling (Eq.5), C_5 in this work could be used directly in full-scale tunnel because C_5 is a function of temperature.

According to the maximum temperature beneath curved ceiling at two representative points (x=4 and 8 cm) in Test 1, 4 and 7, Stanton numbers beneath semicircular ceiling with three kinds of fire plume types were calculated by Eq.22. The outputs as well as C_5 are shown in the Table 4.

Table 4 Summary of Stanton number and other parameters calculated from experiments

Fire plume types at the impingement region	Fuel	St	C_5
Continuous flame	N-heptane	0.0141	0.810
Intermittent flame	Ethanol	0.0127	0.810
plume	Methanol	0.0116	0.810

Seen in the Table 4, it was obvious that Stanton number is influenced by fire plume types at the impingement region, which has been discussed in Eqs.23-24. In addition, the range of calculated Stanton number in this work showed consistent with earlier works [11, 46, 51]. According to the Veldman's study[46], a range of values of Stanton number was given with St = 0.0127 to 0.0254. Delichatsios [11] obtained St =0.03 by comparing the exponential expression he had proposed. Oka et al [51] obtained St = 0.01513 from their experimental study. As a result, comparing with former literature[11, 46, 51], values of Stanton number in this work are acceptable.

Referring to the St and C_5 shown in the Table 4 and Eq.22, the prediction lines (red lines) were calculated to make a comparison with temperature data obtained from Test 1~9 as well as experimental and theoretical outputs in former literature.

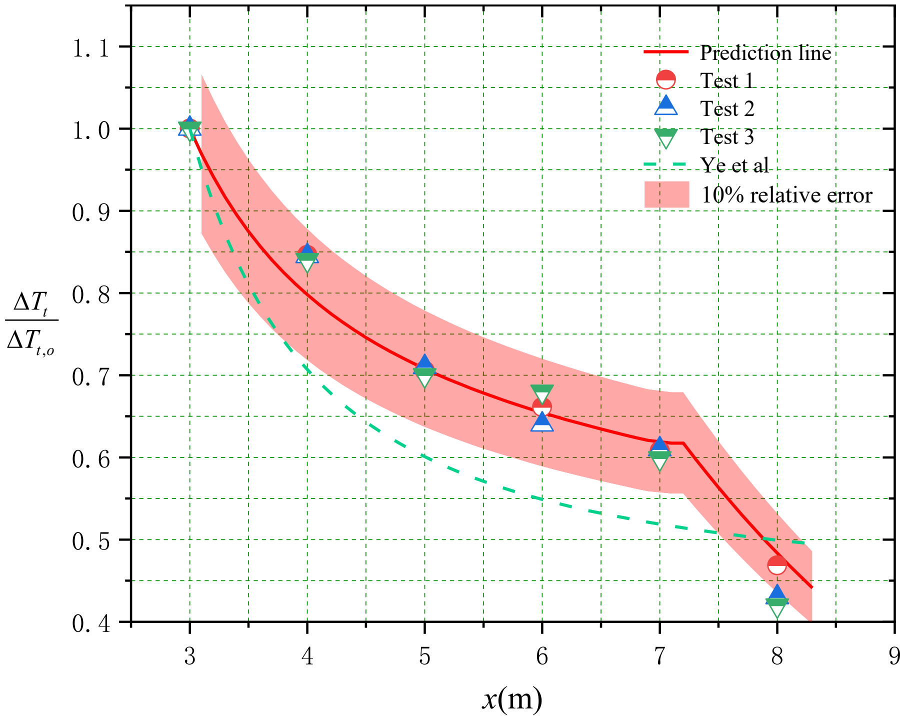

(a) Test 01~03 (continuous flame)

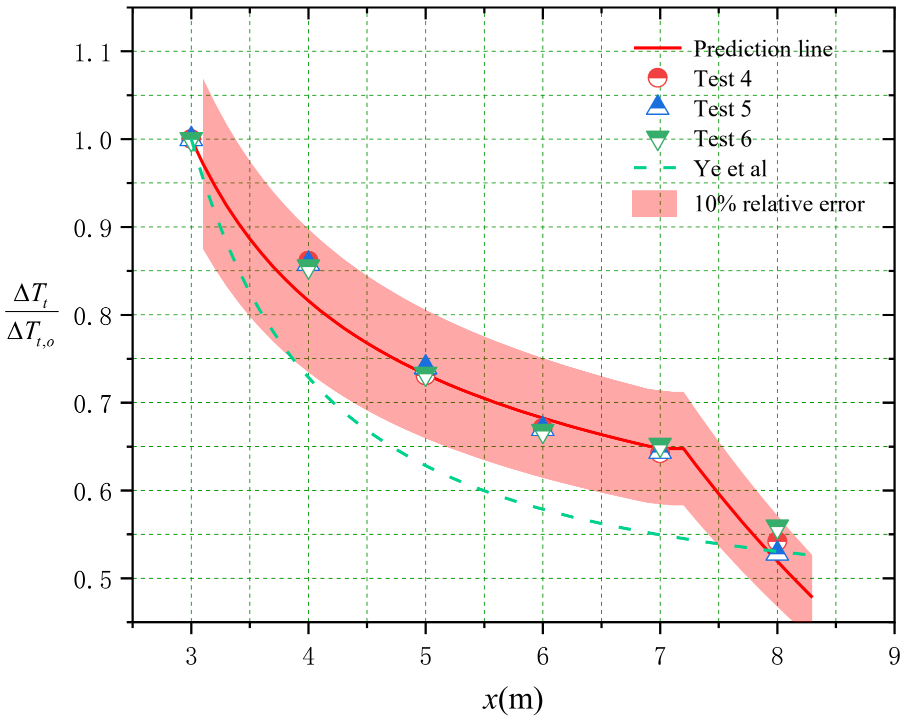

(b) Test 04~06 (intermittent flame)

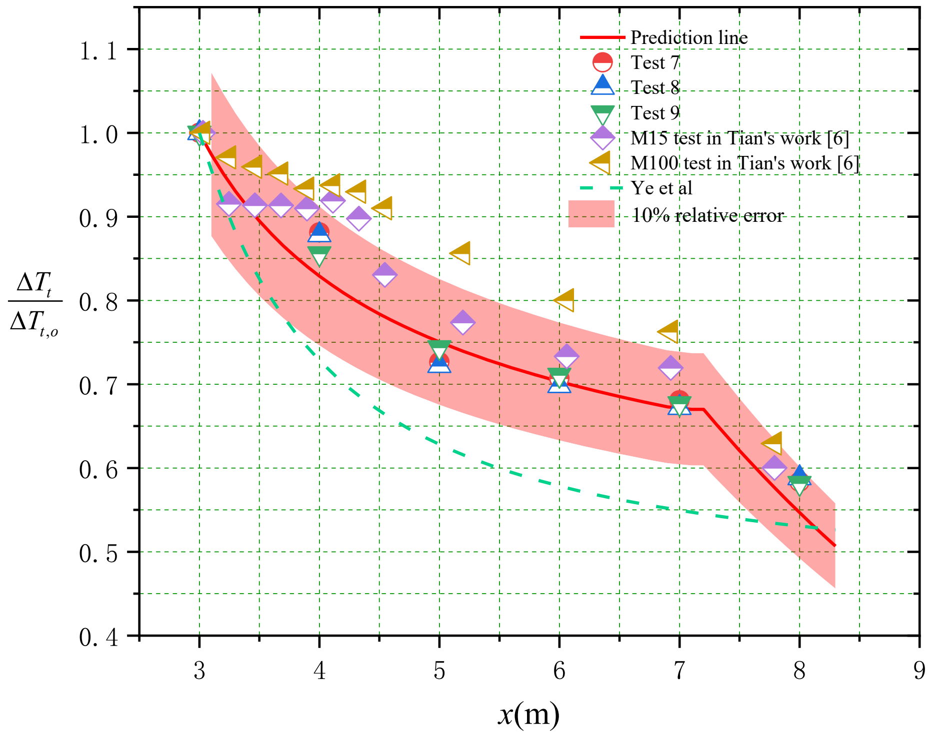

(c) Test 07~09 (plume)

Fig. 11 Comparison between prediction models and experimental data for longitudinal maximum temperature attenuation

As shown in the Fig 11, the prediction lines for longitudinal maximum temperature decay under semicircular ceiling show a good agreement with experiments with within 10% relative error (pink area in the Fig.11). Moreover, proposed models reflect the influence of fire plume types at the impingement region on the temperature decay. Based on the former literature [9, 13, 52-54], the fire plume could be divided into strong and weak plumes. When there is flame existing at the impingement point, the fire plume could be regarded as the strong plume (such as N-heptane and Ethanol in this work), while there is no flame, the fire plume could be defined as weak plume (such as Methanol in this work). Seen in the Fig. 11, obviously, the stronger plume exists in the impingement region, the greater degree of temperature attenuation is predicted.

As reflected in the Fig 11, models (Eq.4) established in the horizontal ceiling were employed to make comparison with models in this work. The Stanton numbers applied to Eq.4 were obtained in their work[13]. Seen in Ye's expression (Eq.4), the predicted value based on Eq.4 was lower than that in this study. This was caused by the difference of control volume selected in Eq.4 and Eq.22. In Ye's work, the cross section of control volume was rectangle while that in this study was semicircular. With the same of thermal boundary thickness $\delta(x)$, wet perimeter of control volume in Ye's work would be larger than that in this work and radiative heat transfer from control volume was also ignored. Therefore, predicted value calculated from Eq.4 shows slightly different from that based on Eq.22.

In addition, as shown in the Fig.11(c), experimental data obtained by former scholar is employed to validate the proposed formular[6]. The experiments were conducted in the full-scale tunnel with semicircle ceiling and the radius of 1.6 m. Considering their work was conducted in the full-scale tunnel with 2.13 times of size in this work, coordinates of the data points were corrected based on the Froude scaling[39]. Seen in the Fig.11(c), the reference point in this work was determined as x=3 m, which corresponds approximately to x=7 m in Tian's work[6]. Temperature data obtained from two representative tests was to make comparison with Eq.22. One group was produced by larger heat release rate and the other was produced by smaller one. It could be noted that trend of data is similar with that of proposed formular (Eq.22). Moreover, majority of data is within the boundary of 10% relative error of Eq.22 (pink area in the Fig.11). The error may be mainly resulted from the measurement in Tian's work. In the reference[6], thermocouples were arranged 10 cm under the ceiling, which means measured values may be not the maximum values near the impingement region. So measured temperature at reference point may be lower than the maximum value, resulting in the reflection in the Fig.11(c).

The proposed model in this work (Eq.22) is only valid under the ceiling with semicircular geometry. It could be applied in the full-scale tunnel based on the Froude scaling (Eq.5). Due to the limitation of experiment, proposed model (Eq.22) could guarantee the accuracy of prediction with $4 \leqslant x/H \leqslant 10.66$.

3.4 Two-dimensional prediction for temperature profile beneath semicircle ceiling centerline

To obtain the two-dimensional temperature profile beneath semicircle ceiling centerline, outputs from section 3.1-3.3 would be used to establish models. According to the Eq.6 and Table 2, the relationship between temperature profile and horizontal positions is described as:

$$\frac{\Delta T(x,z)}{\Delta T_{\max}(x)} = 3.49\left(\frac{z}{L_T}+0.745\right)^{4.90} \exp\left(-4.91\frac{z}{L_T}\right) \tag{25}$$

As mentioned in the section 3.1, L_T represents Gaussian thermal thickness which is defined as the distance from the point where $\triangle T/\triangle T_{max}$ =1/e to ceiling surface. It is the significant parameter when determining the vertical temperature profile. According to the former literature [42, 55], characteristic thermal thicknesses beneath ceiling have the same trend with increasing of x. As a result, it could be inferred that Gaussian thermal thickness L_T in this work could be described by function of x/H and L_T/H, which is similar with the form of Eq.13. However, differ from Eq.13, the Gaussian thermal thickness could not be ignored near x=0 as thermal thickness $\delta(x)$ and formula should make adjustment through adding constant. Based on the experimental data points, Eq.26 was proposed to predict Gaussian thermal thickness under curved ceiling, shown in the Fig.12.

$$L_T / H = \begin{cases} 0.147+0.00123(\dfrac{x}{H})^{2.46} & \text{Region II} \quad (x/H < 9) \\ 0.450(\dfrac{l}{H})^{-1/3} & \text{Region III} \quad (x/H \geq 9) \end{cases} \tag{26}$$

Seen in the Fig.12, Eq.26 could describe the experimental data points within 10% relative error (pink area in the Fig.12). Moreover, data points obtained in former works were employed to make comparison with Eq.26 [55, 56]. These former works were conducted in tunnel with horizonal ceiling and values of experimental data shows a little different with Eq.26 because of different thermal layers distribution between curved ceiling and horizontal one[7]. However, the evolution of Oka's work roughly presents two states, which is similar with evolution in this work. In addition, values of Oka's work near x=0 could be approximately equal to predicted value[56]. Thus, it is reliable that Eq.26 could predict Gaussian thermal thickness under curved ceiling. Considering there is rare literature on Gaussian thermal thickness under curved ceiling, noting could be made a comparison with Eq.26. However, Eq.26 could be applied to the tunnel with semicircular geometry based on the Froude scaling (Eq.5). Meanwhile, it could guarantee the accuracy of prediction with $4 \leqslant x/H \leqslant 10.66$.

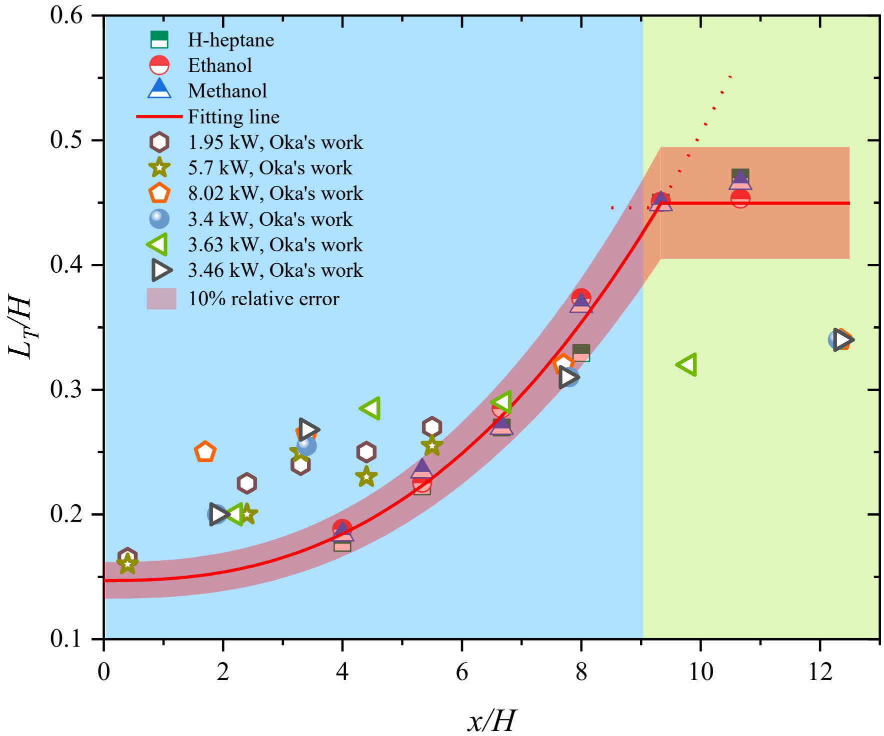

Fig.12 Empirical model for Gaussian thermal thickness beneath curved ceiling

Referring to the maximum temperature at reference point and incorporating Eqs.22, 25-26, the two-dimensional prediction with different fire plume types (continuous flame, intermittent flame and plume) is shown in the Fig.13,

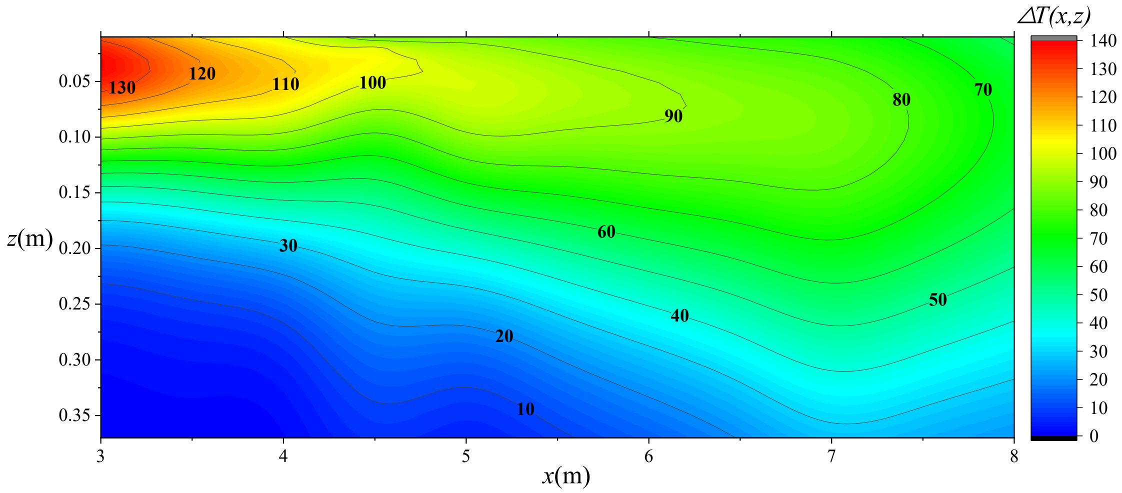

(a) Continuous flame

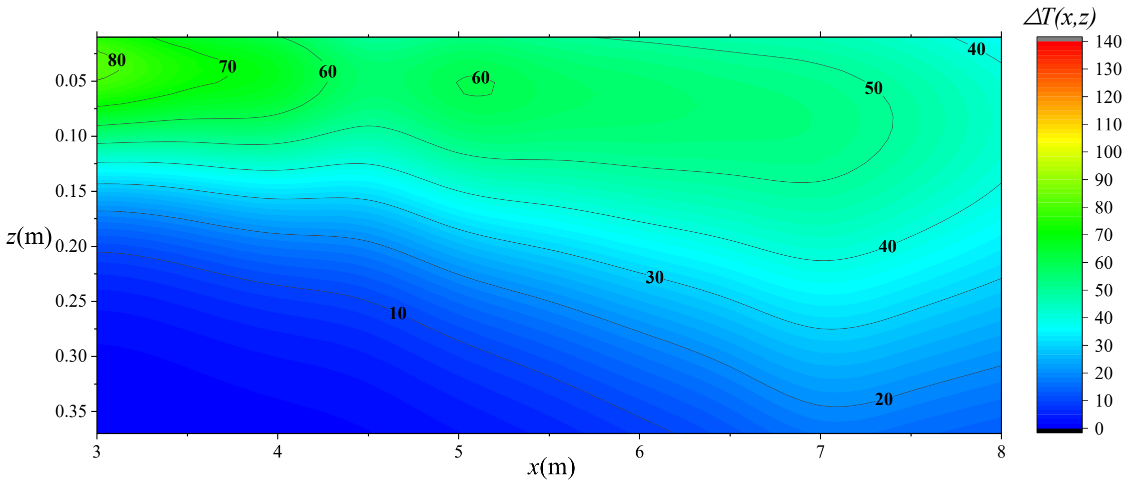

(b) Intermittent flame

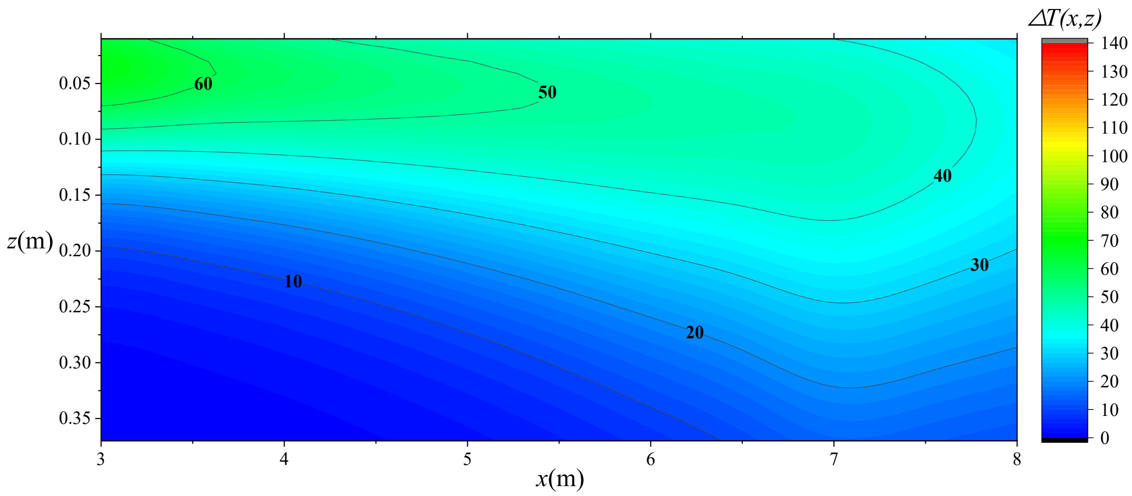

(c) Plume

Fig. 13 Two-dimensional prediction for temperature profile beneath semicircle ceiling centerline

As shown in the Fig.13, it could be roughly determined that predicted two-dimensional temperature distribution shows a good agreement with measured values under semicircular ceiling centerline. In order to make detailed assessment on accuracy of two-dimensional model, all the predicted and measured data points were made a comparison, seen in the Fig.14. It was noted that two-dimensional prediction model could predict majority of measured data within 20% relative error even though some fluctuation. Meanwhile, model perform well in high temperature rise region, comparing with lower temperature rise region. However, after eliminating fluctuation caused by measurement error, the two-dimensional prediction model could be applied to the fire protection engineering in semicircular tunnel. In addition, considering that the limitation of experiments and analysis, two-dimensional prediction is valid with $4 \le x/H \le 10.66$. For more application range, lager scale experiments are required.

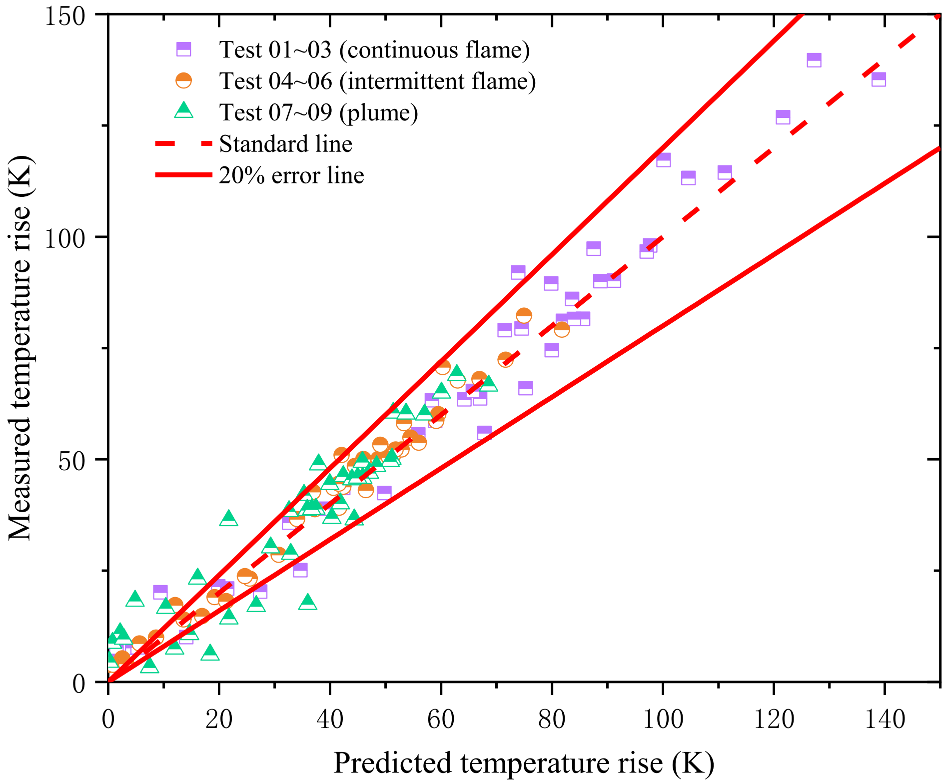

Fig.14 Comparison of experimental and predicted values

Conclusion

This paper presented a series of experimental studies and theoretical analysis on the temperature profile, thermal boundary layer thickness and longitudinal temperature distribution beneath ceiling centerline in semicircular tunnel. The major conclusions are as follows:

(1) The relationship between vertical temperature profile beneath curved ceiling and vertical distance from the ceiling could be unified in a dimensionless form regardless of horizontal positions. Meanwhile, it is found that vertical temperature profile under curved ceiling shows lower temperature gradient than that under horizontal ceiling in the region $0 < z < z_{max}$. Through theoretical analysis, curved geometry reduces the average velocity of ceiling jet, resulting in the lower heat transfer coefficient of ceiling jet under the curved ceiling. This determines less heat transfer from ceiling jet to ceiling surface, causing lower temperature gradient under curved ceiling.

(2) Referring to the former literature, the evolution of thermal boundary layer thickness was divided into two regions based on the experimental temperature data. Models (Eq.13) for thermal boundary layer thickness in these two regions are established in terms of horizontal distance from fire source, half width and ceiling clearance. With the same method, evolution of Gaussian

thermal thickness under curved ceiling is also described by the empirical model (Eq.26). It is found that both thermal layer thickness and Gaussian thermal thickness are independent of fire plume types at the impingement region.

⑶ According to the model for thermal layer thickness, conservation equations in thermal layer are established to describe the temperature attenuation of thermal layer beneath semicircular ceiling. With these conservation equations, prediction models (Eq.22) for the longitudinal temperature distribution beneath ceiling were proposed. Comparing with experiments and former literature, prediction lines show a good agreement with trend proposed by former literature and this work with 10%. relative error.

⑷ Two -dimensional prediction for temperature profile beneath semicircle ceiling centerline was proposed from works on vertical temperature profile (Eq.25), thermal boundary layer thickness (Eq.13), Gaussian thermal thickness (Eq.26) and longitudinal maximum temperature attenuation (Eq.22). After validation, prediction model could predict majority of measured data within 20% relative error.

Acknowledgements

The work was supported by the National Key Research and Development Program of China (No.2016YFC0802900) and Graduate Research and Innovation Projects of Jiangsu Province (KYCX21_2446). Also, authors would like to thank the China Scholarship Council (CSC) for the financial support of the first author (Grant No. 202006420046).

Conflicts of interest/Competing interests

The authors declared that they have no conflicts of interest to this work. We declare that we do not have any commercial or associative interest that represents a conflict of interest in connection with the work submitted.

Availability of data and material

The datasets used during the current study are available from the corresponding author on reasonable request.

Code availability

Not applicable

Appendix

Based on the flow mechanisms of the thermal boundary layer described in the Fig 5, referring to the former literature [13, 35, 41, 43], governing equations of a differential volume in one-dimensional thermal boundary layer were established. There are several assumptions:

①Steady HRR;

②The properties of thermal layer in one-dimensional ceiling jet is stable, such as density, velocity;

③There would be hardly any mass exchange in smoke layer except for entrainment.

With assumptions mentioned above, governing equations for selected control volume are shown as follows:

Continuity equation,

$$\dot{m}_e = \frac{d\dot{m}}{dx} \tag{A1}$$

Energy conservation equation,

$$\frac{d(C_p \dot{m} T_t)}{dx} = C_p \dot{m}_e T_e - Q_{conv} - Q_{rad} \tag{A2}$$

The relationship between dT_t and dx is expected to obtained from conservation equations mentioned above. As the boundary for Eq.A1, mass flow equation is expressed,

$$\dot{m} = \rho u s \tag{A3}$$

As shown in the Eqs.A1-A3, $\dot{m}$ and $\dot{m}_e$ represented the mass flow of thermal layer and entrained flow, respectively. The mass flow of thermal layer is described by the smoke density ρ, horizontal flow velocity of thermal layer u and cross-section area of thermal boundary layer s. In addition, Q_{conv} and Q_{rad} are the convective and radiative heat loss from thermal layer to the ceiling, respectively. Considering that fire duration is short in comparison to thermal inertia of concrete in this work, the temperature of concrete wall T_w far from fire source was assumed as that of ambient air T_∞. As a result, Q_{conv} and Q_{rad} could be written as:

$$Q_{conv} = h_c B (T_t - T_\infty) \tag{A4}$$

$$Q_{rad} = \varepsilon \sigma B (T_t^4 - T_\infty{}^4) = \varepsilon \sigma B (T_t^2 + T_\infty{}^2)(T_t + T_\infty)(T_t - T_\infty) \tag{A5}$$

Based on the reference[45, 57, 58], radiative heat transfer coefficient would be employed in the Eq.A5, which has the same dimension with convective heat transfer coefficient. The Eq.A5 could be transformed as:

$$Q_{rad} = h_{rad} B(T_t - T_\infty) \tag{A6}$$

Incorporating Eqs.A1-A6, a new equation was obtained,

$$C_p \frac{dT_t}{dx}\dot{m} + C_p \frac{d\dot{m}}{dx} T_t = C_p \frac{d\dot{m}}{dx} T_e - h_c B(T_t - T_\infty) - h_{rad} B(T_t - T_\infty) \tag{A7}$$

To simplify the one-dimensional model, on the basic of assumptions, the characteristic temperature of thermal layer T_t was equal to that of entrained layer T_e. Thus Eq.A7 was expressed as follows:

$$-\frac{dT_t}{T_t - T_\infty} = \frac{(h_c + h_{rad})B}{C_p \rho u s} dx \tag{A8}$$

Reference

1. Tang F, Zhao Z, Zhao K (2020) Experimental investigation on carriage fires hazards in the longitudinal ventilated tunnels: Assessment of the smoke stratification features. Safety Science 130: 104901 DOI https://doi.org/10.1016/j.ssci.2020.104901
2. Gong L, Jiang L, Li S, Shen N, Zhang Y, Sun J (2016) Theoretical and experimental study on longitudinal smoke temperature distribution in tunnel fires. International Journal of Thermal Sciences 102: 319-328 DOI https://doi.org/10.1016/j.ijthermalsci.2015.12.006
3. Pan R, Zhu G, Liang Z, Zhang G, Liu H, Zhou X (2020) Experimental study on the fire shape and maximum temperature beneath ceiling centerline in utility tunnel under the effect of curved sidewall. Tunnelling and Underground Space Technology 99: 103304 DOI https://doi.org/10.1016/j.tust.2020.103304
4. Wang P, Zhu G, Pan R, Chu T, Wang Z, Liu H (2020) Effects of curved sidewall on maximum temperature and longitudinal temperature distribution induced by linear fire source in utility tunnel. Case Studies in Thermal Engineering 17: 100555 DOI https://doi.org/10.1016/j.csite.2019.100555
5. Zhou X, Zhu G-q, Liu H-n, Liang Z-h (2019) Experimental investigation on the influence of linear fire source along the wall on the temperature distribution in tunnel. Case Studies in Thermal Engineering 14: 100473 DOI https://doi.org/10.1016/j.csite.2019.100473
6. Tian X, Zhong M, Shi C, Zhang P, Liu C (2017) Full-scale tunnel fire experimental study of fire-induced smoke temperature profiles with methanol-gasoline blends. Applied Thermal Engineering 116: 233-243 DOI https://doi.org/10.1016/j.applthermaleng.2017.01.099
7. Zhou T, Zhou Y, Fan C, Wang J (2020) Experimental study on temperature distribution beneath an arced tunnel ceiling with various fire locations. Tunnelling and Underground Space Technology 98: 103344 DOI https://doi.org/10.1016/j.tust.2020.103344
8. Pan R, Zhu G, Xu G, Liu X (2021) Experimental analysis on burning rate and temperature profile produced by pool fire in a curved tunnel as a function of fire location. Process Safety and Environmental Protection 152: 549-567 DOI https://doi.org/10.1016/j.psep.2021.06.039
9. Zhou TN, He YP, Lin X, Wang XH, Wang J (2017) Influence of constraint effect of sidewall on maximum smoke temperature distribution under a tunnel ceiling. Applied Thermal

Engineering 112: 932-941 DOI 10.1016/j.applthermaleng.2016.10.111
10. Alpert RL (1975) Turbulent ceiling-jet induced by large-scale fires. Combustion Science and Technology 11: 197-213
11. Delichatsios MA (1981) The flow of fire gases under a beamed ceiling. Combustion and Flame 43: 1-10 DOI https://doi.org/10.1016/0010-2180(81)90002-X
12. Ingason H, Ying ZL, Lönnermark A (2015) Tunnel Fire Dynamics
13. Ye K, Zhou X, Zheng Y, Liu H, Tang X, Cao B, Huang Y, Chen Y, Yang L (2019) Estimating the longitudinal maximum gas temperature attenuation of ceiling jet flows generated by strong fire plumes in an urban utility tunnel. International Journal of Thermal Sciences 142: 434-448
14. Zheng Y, Zhou XD, Chen YQ, Cao B, Huang YB, Ye K, Yang LZ (2017) A study on the temperature distribution based on the smoke thermal boundary layer below ceiling in the locomotive. Applied Thermal Engineering 127: 776-788 DOI 10.1016/j.applthermaleng.2017.08.075
15. Shi C, Li J, Xu X (2021) Full-scale tests on smoke temperature distribution in long-large subway tunnels with longitudinal mechanical ventilation. Tunnelling and Underground Space Technology 109: 103784 DOI https://doi.org/10.1016/j.tust.2020.103784
16. Oka Y, Oka H, Imazeki O (2016) Ceiling-jet thickness and vertical distribution along flat-ceilinged horizontal tunnel with natural ventilation. Tunnelling and Underground Space Technology 53: 68-77 DOI https://doi.org/10.1016/j.tust.2015.12.019
17. Tang F, Mei FZ, Wang Q, He Z, Fan CG, Tao CF (2017) Maximum temperature beneath the ceiling in tunnel fires with combination of ceiling mechanical smoke extraction and longitudinal ventilation. Tunnelling and Underground Space Technology 68: 231-237 DOI https://doi.org/10.1016/j.tust.2017.05.029
18. Li YZ, Lei B, Ingason H (2011) The maximum temperature of buoyancy-driven smoke flow beneath the ceiling in tunnel fires. Fire Safety Journal 46: 204-210 DOI 10.1016/j.firesaf.2011.02.002
19. Tang F, Li LJ, Dong MS, Wang Q, Mei FZ, Hu LH (2017) Characterization of buoyant flow stratification behaviors by Richardson (Froude) number in a tunnel fire with complex combination of longitudinal ventilation and ceiling extraction. Applied Thermal Engineering 110: 1021-1028 DOI doi.org/10.1016/j.applthermaleng.2016.08.224
20. Chen C, Zhang Y, Lei P, Jiao W (2020) A study for predicting the maximum gas temperature beneath ceiling in sealing tactics against tunnel fire. Tunnelling and Underground Space Technology 98: 103275 DOI https://doi.org/10.1016/j.tust.2019.103275
21. Ishikawa T, Kasumi K, Tanaka F, Moinuddin KAM (2020) Combustion efficiency during fires in tunnels with natural ventilation by vitiated air including descending smoke. Fire Safety Journal: 103093 DOI https://doi.org/10.1016/j.firesaf.2020.103093
22. Yao Y, Li YZ, Ingason H, Cheng X (2019) Scale effect of mass loss rates for pool fires in an open environment and in tunnels with wind. Fire Safety Journal 105: 41-50 DOI https://doi.org/10.1016/j.firesaf.2019.02.004
23. Liang Z-h, Zhu G-q, Liu H-n, Zhou X (2019) Flame characteristic and ceiling temperature distribution under the effect of curved sidewall. Case Studies in Thermal Engineering 14: 100453
24. Huang Y, Li Y, Li J, Dong B, Bi Q, Li Y, Li J (2019) Experimental investigation on temperature profile with downstream vehicle in a longitudinally ventilated tunnel.

Experimental Thermal and Fluid Science 103: 149-156
25. Yao Y, He K, Peng M, Shi L, Cheng X, Zhang H (2018) Maximum gas temperature rise beneath the ceiling in a portals-sealed tunnel fire. Tunnelling and Underground Space Technology 80: 10-15
26. Silvani X, Morandini F (2009) Fire spread experiments in the field: Temperature and heat fluxes measurements. Fire Safety Journal 44: 279-285 DOI https://doi.org/10.1016/j.firesaf.2008.06.004
27. Welch S, Jowsey A, Deeny S, Morgan R, Torero JL (2007) BRE large compartment fire tests—Characterising post-flashover fires for model validation. Fire Safety Journal 42: 548-567 DOI https://doi.org/10.1016/j.firesaf.2007.04.002
28. Blevins LG, Pitts WM (1999) Modeling of bare and aspirated thermocouples in compartment fires. Fire Safety Journal 33: 239-259 DOI https://doi.org/10.1016/S0379-7112(99)00034-X
29. Mingchun L (1997) Effects of Radiation on Temperature Measurement in a Fire Environment. Journal of Fire Sciences 15: 443-461 DOI 10.1177/073490419701500602
30. Oka Y, Imazeki O (2014) Temperature and velocity distributions of a ceiling jet along an inclined ceiling - Part 1: Approximation with exponential function. Fire Safety Journal 65: 41-52 DOI 10.1016/j.firesaf.2013.07.009
31. Oka Y, Imazeki O (2014) Temperature and velocity distributions of a ceiling jet along an inclined ceiling-Part 2: Approximation based on cubic function and coordinate transformation. Fire Safety Journal 65: 53-61 DOI 10.1016/j.firesaf.2014.02.006
32. Oka Y, Imazeki O (2015) Temperature distribution within a ceiling jet propagating in an inclined flat-ceilinged tunnel with natural ventilation. Fire Safety Journal 71: 20-33
33. Motevalli V, Marks CH (1991) Characterizing the unconfined ceiling jet under steady-state conditions: a reassessment. Fire Safety Science 3: 301-312
34. Alpert RL (2016) Ceiling Jet Flows. In: Hurley MJ, Gottuk D, Hall JR, Harada K, Kuligowski E, Puchovsky M, Torero J, Watts JM, Wieczorek C (eds) SFPE Handbook of Fire Protection Engineering Springer New York, New York, NY, pp. 429-454.
35. Guo Q, Li YZ, Ingason H, Yan Z, Zhu H (2020) Theoretical studies on buoyancy-driven ceiling jets of tunnel fires with natural ventilation. Fire Safety Journal: 103228 DOI https://doi.org/10.1016/j.firesaf.2020.103228
36. Glauert M (1956) The wall jet. Journal of Fluid mechanics 1: 625-643
37. Bakke P (1957) An experimental investigation of a wall jet. Journal of Fluid Mechanics 2: 467-472
38. Schwarz W, Cosart W (1961) The two-dimensional turbulent wall-jet. Journal of Fluid mechanics 10: 481-495
39. Li YZ, Ingason H (2013) Model scale tunnel fire tests with automatic sprinkler. Fire Safety Journal 61: 298-313
40. Yang D, Hu LH, Huo R, Jiang YQ, Liu S, Tang F (2010) Experimental study on buoyant flow stratification induced by a fire in a horizontal channel. Applied Thermal Engineering 30: 872-878 DOI https://doi.org/10.1016/j.applthermaleng.2009.12.019
41. Kunsch J (1998) Critical velocity and range of a fire-gas plume in a ventilated tunnel. Atmospheric Environment 33: 13-24
42. Ye K, Tang X, Zheng Y, Ju X, Peng Y, Liu H, Wang D, Cao B, Yang L (2021) Estimating the two-dimensional thermal environment generated by strong fire plumes in an urban utility

tunnel. Process Safety and Environmental Protection 148: 737-750 DOI https://doi.org/10.1016/j.psep.2021.01.030
43. Hu LH (2006) Studies on thermal physics of smoke movement in tunnel fires University of Science and Technology of China.
44. Liu H, Zhu G, Liang Z, Zhou X (2019) Experimental Study of Smoke Deposition in the Case of Leakage Joint at the Bottom of Circular Utility TunnelIOP Conference Series: Earth and Environmental Science IOP Publishing, pp. 012099.
45. Karadağ R (2009) The investigation of relation between radiative and convective heat transfer coefficients at the ceiling in a cooled ceiling room. Energy Conversion and Management 50: 1-5 DOI https://doi.org/10.1016/j.enconman.2008.09.008
46. Veldman C, Kubota T, Zukoski E (1975) An experimental investigation of the heat transfer from a bouyant gas plume to a horizontal ceiling. Part 1: Unobstructed ceiling. cit
47. Karlsson B, Quintiere J (1999) Enclosure fire dynamics CRC press
48. Pan R, Zhu G, Zhang G, An W, Zhu H, Yu M (2019) Experimental study and heat transfer analysis of downward flame spread over PMMA under the effect of wall spacing. Journal of Thermal Analysis and Calorimetry 138: 1711-1722 DOI 10.1007/s10973-019-08119-6
49. Incropera FP (1985) Fundamentals of Heat and Mass Transfer Wiley
50. Walton GN (1980) A new algorithm for radiant interchange in room loads calculations
51. Oka Y, Oka H (2016) Velocity and temperature attenuation of a ceiling-jet along a horizontal tunnel with a flat ceiling and natural ventilation. Tunnelling and Underground Space Technology 56: 79-89 DOI 10.1016/j.tust.2016.03.001
52. Zhou T, Chen Q, Wang X, Zhao J, Ding C, Wang J (2018) The burning rate of n-heptane pool fires with constraint effect beneath an arced ceiling. Fuel 233: 825-833 DOI https://doi.org/10.1016/j.fuel.2018.07.001
53. Tiannian Zhou HL, Qinpei Chena, Ruichao Weia, Jian Wanga, (2018) Understanding sidewall constraint involving ventilation effects on temperature distribution of fire-induced thermal flow under a tunnel ceiling. International Journal of Thermal Sciences 129: 290-300
54. Gao Z, Jie J, Wan H, Zhu J, Sun J (2017) Experimental investigation on transverse ceiling flame length and temperature distribution of sidewall confined tunnel fire. Fire Safety Journal 91: 371-379
55. Oka Y, Oka H, Imazeki O (2014) Experimental study on temperature property along a tunnel axis with flat ceiling in natural ventilation. Fire Safety Science 11: 472-485
56. Oka Y, Kakae N, Imazeki O, Inagaki K (2013) Temperature Property of Ceiling Jet in an Inclined Tunnel. Procedia Engineering 62: 234-241 DOI https://doi.org/10.1016/j.proeng.2013.08.060
57. Li S, Zong R, Zhao W, Yan Z, Liao G (2011) Theoretical and experimental analysis of ceiling-jet flow in corridor fires. Tunnelling and Underground Space Technology 26: 651-658 DOI https://doi.org/10.1016/j.tust.2011.05.011
58. Evangelisti L, Guattari C, Gori P, Bianchi F (2017) Heat transfer study of external convective and radiative coefficients for building applications. Energy and Buildings 151: 429-438 DOI https://doi.org/10.1016/j.enbuild.2017.07.004